Title

Beta2* Nicotinic Receptors Tune Prefrontal Behavior Through Distinct Neuronal Populations

Authors

Alice Abbondanza[1, 2], Jan Elias[3], Chandani R. Verma[1], Amanda Rosanna Alves Barboza[1], Martin Capek[4, 5], Trisha Jigar Dhabalia[1], Andrea Grigelova[6], Sylvie Dumas[7], Veronique Bernard[2], Helena Janickova[1]

Affiliations

[1], Laboratory of Cholinergic Signaling, Institute of Physiology of the Czech Academy of Sciences, Prague, 14200, Czech Republic

[2], Neuroscience at Sorbonne Université (NeuroSU), Institut de Biologie Paris Seine, Institut National de la Santé et de la Recherche Médicale, Centre National de la Recherche Scientifique, Sorbonne Université, Paris, 75005, France

[3], Institute of Molecular Genetics of the Czech Academy of Sciences, Czech Centre for Phenogenomics, Vestec, Czech Republic

[4], Laboratory of Advanced Microscopy and Data Analysis, Institute of Physiology of the Czech Academy of Sciences, Prague, 14200, Czech Republic

[5], Light Microscopy, Institute of Molecular Genetics of the Czech Academy of Sciences, Prague, 14200, Czech Republic

[6], Laboratory of Developmental Epileptology, Institute of Physiology of the Czech Academy of Sciences, Prague, 14200, Czech Republic

[7], Oramacell, Paris, 75006, France

Abstract

Nicotinic acetylcholine receptors containing beta2 subunit (beta2* nAChRs) are widely expressed in the mouse prefrontal cortex (PFC), where they regulate behavioral and cognitive domains associated with this region and represent potential therapeutic targets for neuropsychiatric symptoms. However, current pharmacological tools cannot distinguish among receptors expressed by different neuronal populations, and the functional roles of beta2* nAChRs in specific neuronal types remain poorly understood. In this study, we examined the expression and behavioral significance of beta2* nAChRs in distinct neuronal populations of the mouse PFC. We first used fluorescence in situ hybridization (FISH) to analyze the expression of the beta2 nicotinic subunit in major neuronal types and cortical layers. We then used CRISPR to knock down (KD) the beta2 subunit in two PFC populations and, for comparison, in a striatal population. KD of the beta2 subunit in deep-layer PFC neurons defined by neuropeptide Y (NPY) expression specifically altered working memory and exploratory behavior and affected social and anxiety-like behavior. In contrast, KD in PFC interneurons expressing serotonin receptor 5HT3a led to a hypersocial phenotype. KD of beta2* nAChRs in a rare NPY-expressing striatal population resulted in subtler and largely opposing changes in similar behavioral domains. These findings show that beta2* nAChRs expressed by distinct neuronal populations contribute differentially, and sometimes oppositely, to behavioral regulation. Our data suggest that cell-type- and region-specific expression of beta2* nAChRs is required for the modulation and fine-tuning of behavioral domains relevant to neuropsychiatric disorders.

Introduction

Neuronal nicotinic acetylcholine receptors (nAChRs) are pentameric ion channels composed of 12 subunits (α2-10, β2-4). Among them, heteromeric alpha4beta2* receptors (asterisk indicating that additional subunits may be part of the pentamer) (1,2) are one of the most common nicotinic subtypes in the mammalian brain. They regulate fundamental neuronal processes, including neurotransmitter release, excitability and plasticity (3,4). Their wide expression and essential physiological roles make them attractive therapeutic targets (5).

The rodent prefrontal cortex (PFC) has been implicated in critical cognitive and behavioral domains, including attention, memory, social interactions, and anxiety- and depression-like behaviors. These functions depend on complex signaling across diverse neuronal types that differ in morphology, gene expression, electrophysiological properties and circuit connectivity (6–8). Many of these PFC neuronal populations express beta2-containing nAChRs (beta2* nAChRs) (8), and the contribution of prefrontal beta2* nAChRs to cognitive and behavioral regulation is well established (9,10).

Despite substantial research on beta2* nAChRs in the PFC, a detailed understanding of their expression across individual neuronal types is still lacking (6,11,12). Most available information comes from electrophysiological studies that, while highly informative, do not provide population-level quantification. Likewise, most genetic and pharmacological manipulations to date have targeted the PFC globally or at the level of large anatomical subregions (11,13,14), limiting insight into the cell-type-specific contributions of beta2* nAChRs to behavior. By contrast, the functional relevance of beta2* nAChRs expressed in defined neuronal populations remains much less explored (15). This gap has become increasingly important as modern molecular approaches reveal extensive neuronal diversity, highlighting the possibility that perturbing the same receptor subtype in different neuronal classes may produce distinct circuit and behavioral effects.

In this study, we address this gap by elucidating the expression and functional role of beta2* nAChRs in defined PFC neuronal populations. First, we performed a systematic analysis of beta2 subunit expression across individual neuronal types and cortical layers of the PFC. We then focused on two neuronal populations that differ markedly in abundance, laminar localization and functional properties (16,17): neurons expressing neuropeptide Y (NPY) and interneurons expressing the serotonin receptor 5HT3a. Our primary goals were to determine whether

knockdown (KD) of the beta2 subunit in these populations produces detectable and reproducible behavioral changes and to assess whether the consequences differ between the two populations. For regional comparison, we also examined the effects of beta2 KD in NPY-positive neurons of the dorsal striatum. All KD mutants were subjected to comprehensive behavioral testing targeting domains strongly linked to PFC function and commonly altered in neuropsychiatric disorders, thereby probing the therapeutic relevance of beta2* nAChRs expressed by specific neuronal types.

Methods and Materials

Animals

All procedures followed the European Community Council directive for laboratory animal use (2010/63/EU) and were approved by the Ethics Committee for animal experimentation of the Czech Academy of Sciences. Only male mice were used due to resource limitations. Tissue for FISH, qPCR, T7 assay and radioligand binding was collected from 2-3-month-old mice. The following lines were used: C57BL/6 wild-type (WT) mice; beta2-flox/flox mice (18) carrying floxed exon 5 of *Chrnb2*; Rosa26-floxed STOP-Cas9 knock-in mice with Cre-inducible Cas9-2A-EGFP expression (19); and two Cre-driver lines expressing Cre under the Npy or Htr3a promoters (20,21). Details of all lines are provided in Supplementary Table S1.

Experimental design and statistical analysis

Mice were semi-randomly assigned so that each cage contained animals from both control and experimental groups. To assess reproducibility, selected behavioral experiments were performed in two independent cohorts originating from different housing facilities and tested more than 12 months apart. Behavioral outliers were defined as values exceeding the mean ± 2 SD and were removed from all parameters within that experiment. After behavioral testing, brains were examined for AAV expression; animals lacking expression were excluded. Statistical analyses were performed in GraphPad Prism (version 10). Two-tailed t-tests were used for comparison between two groups, and two-way ANOVA with Sidak's post-hoc test was used for analyses involving two variables. All graphs show mean ± SEM.

Double-probe fluorescence in situ hybridization (FISH)

FISH was performed as previously reported (22,23). Brains were sectioned at 16 µm thickness. Digoxigenin (DIG)- or fluorescein-labelled RNA probes were synthesized using in vitro transcription with labelled nucleotides (Sigma-Aldrich; Reference 11277073910 and 11685619910). Sections were fixed in 4 % paraformaldehyde (PFA) and acetylated in 0.25 % acetic anhydride/100 mM triethanolamine. Hybridization was performed for 18 h at 65 °C in formamide buffer containing 1 µg/ml of each riboprobe. Sections were washed in decreasing-strength SSC buffers at 65 °C and blocked with 20 % fetal bovine serum (FBS) and 1 % blocking solution. DIG was detected with HRP-anti-DIG Fab fragments (1:2500; Sigma-Aldrich; Reference 11207733910) and visualized with Cy3-tyramide (1:100). Fluorescein was detected with HRP-anti-fluorescein Fab fragments (1:5000; Sigma-Aldrich; Reference 11426346910) and revealed using Cy2-tyramide (1:250). Slides were scanned at 20x resolution using a NanoZoomer 2.0-HT system (Hamamatsu, Japan), and images were analyzed with NDP.view2 (Hamamatsu Photonics) and QuPath (24). Regions of interest were defined using the Paxinos atlas (25).

Quantitative PCR (qPCR)

RNA was extracted using TriPure reagent (Roche), DNase-treated, and reverse-transcribed using LunaScript RT SuperMix (NEB). qPCR was performed using gb SG PCR Master mix (Generi Biotech).

AAV vectors and CRISPR/Cas9 gene editing

AAV-U6-sgRNA-hSyn-mCherry vectors expressed single guide RNA (sgRNA) (Addgene #87916). We used a previously validated (26) sgRNA targeting (sequence: ATCAGCTTGTTATAGCGGGA) and a scrambled control sgRNA (GCGAGGTATTCGGCTCCGCG). The sgRNA was expressed from the U6 promoter, and mCherry from the hSyn promoter. Cloning followed established protocols (27). Vectors were packaged into the AAV5 (UNC Vector Core) at titers of $1 \times 10^{12\text{-}13}$ vg/ml.

Stereotaxic surgeries

Mice were anesthetized with ketamine/xylazine (Vetoquinol, bioveta). PFC stereotaxic coordinates were AP +2.5/+2.2, ML±0.4/±0.3, DV -1.9/-2.1. Dorsal striatum (DS) coordinates were AP +1.4, ML ±1.6, DV -3.5/-2.6. Injections (500 nl each)were made using a microinjection pump (MICRO-2T-UMP3-NL2010, World Precision Instruments) at 50 nl/min. AAV expression

was verified via mCherry fluorescence. Double-positive cells were counted in sections spaced by 0.2 mm apart from +2.8 to +1.6 relative to bregma.

Radioligand binding with [3H]epibatidine

Membranes were prepared from PFC tissue expressing AAV vectors. NPY-Cre::Cas9-GFP mice were injected with sgRNA-Chrnb2 or control sgRNA-scr; beta2-flox/flox mice received AAV5-CMV-Cre-GFP or AAV5-CMV-GFP. To maximize labeled tissue, three injections (500 nl each) were made across AP +2.8/+2.4/+2.0, ML 0, and DV -1.5/-2.0/-2.2. Three weeks later, tissue showing fluorescence was dissected, homogenized in PBS with protease inhibitors, and centrifuged. Protein concentration was measured via Lowry's assay (28). Membrane homogenates were incubated with 0.2 nM [3H]epibatidine (62.2 Ci/mmol, Perkin-Elmer) overnight at 4 °C. Samples were filtered through polyethyleneimine-soaked GFC filters, and radioactivity was measured with a scintillation counter (Tri-Carb, Perkin-Elmer).

T7 endonuclease assay

The assay followed the manufacturer's instructions (T7 Endonuclease Detection Assay Kit, Sigma-Aldrich). Tissue was collected from three sgRNA-Chrnb2-injected NPY-Cre::Cas9 mice, two sgRNA-scr controls, and one non-injected mouse. DNA was extracted by phenol-chloroform. The targeted Chrnb2 region was amplified using Phusion High-Fidelity polymerase (ThermoFisher), denatured, reannealed, and digested with T7 endonuclease to detect CRISPR-induced mismatches.

Behavioral testing

The behavioral tests were performed in the following order: the open field (OF) test, social preference test, social memory test (omitted in Htr3a-Cre::Cas9-GFP mice), hole-board test, Y-maze spontaneous alternations test, novel object recognition (NOR) test, light/dark test, tail suspension test (TST), elevated plus maze (EPM), social interaction (SI) and the forced swim test (FST). All tests except the light/dark test were conducted during the light phase of the light/dark cycle, in a dedicated testing room. The details on the individual test can be found in the Supplementary material.

Results

Analysis of beta2* nAChRs expression in specific neuronal types in the mouse PFC

We first used FISH to analyze *Chrnb2* expression in major PFC neuronal populations (Fig. 1A). Across bregma levels (+2.8-+1.6), *Chrnb2* expression was stable (Suppl. Fig. S1A). Layer analysis showed fewer *Chrnb2*+ cells in layer I than in all other layers, with no major differences elsewhere (Suppl. Fig. S1B). We then examined *Chrnb2* expression in excitatory *Vglut1*+ neurons and in five inhibitory populations: neuropeptide Y-positive (*Npy*+), vasoactive intestinal peptide-positive (*Vip*+), serotonin receptor 5HT3a-positive (*Htr3a*+), parvalbumin-positive (*Pv*+) and somatostatin-positive (*Sst*+) neurons (Fig. 1B-D). Their distribution was layer-dependent and matched published data (29,30); *Vip*+ and *Htr3a*+ neurons were enriched in the superficial layers, whereas the others predominated in deeper layers (Fig. 1E-G).

Then we examined the proportion of *Chrnb2*+ cells in each population. Surprisingly, layer had little effect on the percentage of *Chrnb2*+ cells within each population, except for *Vip*+ neurons, which showed increased expression in layer VI (Suppl. Fig. 1D). Therefore, we averaged the data across layers (Fig. 1H). All neuronal types expressed *Chrnb2*, with the highest levels in *Pv*+ neurons (nearly all *Pv*+ cells), followed by *Vglut1*+ neurons (~80 %). *Npy*+ and *Htr3a*+ populations showed similar expression (~70 %), while *Vip*+ neurons expressed *Chrnb2* least (~50 %) (Fig. 1H). We also quantified the contribution of each population to total *Chrnb2* expression (Fig. 1I). It was mostly dependent on their overall layer distribution, with the notable exception of *Vip*+ neurons in layer VI (see above), which increased their contribution due to the higher *Chrnb2* expression in that layer (Fig. 1I, Suppl. Fig. S1C). In addition, in layer VI, nearly all Chrnb2+ cells belonged to the examined types, whereas in superficial layers, *Chrnb2*+ cells exceeded their combined contribution. It suggests additional unprofiled cell types contributing to *Chrnb2* expression in the upper layers. Overall, *Chrnb2* mRNA was detected in most PFC neurons, with population identity more influential than layer localization.

CRISPR KD of the beta2 nicotinic subunit in NPY-Cre expressing neurons

Given the widespread expression of beta2* nAChRs, we next tested whether selective KD in a single neuronal population would yield reproducible behavioral effects. We chose NPY-expressing neurons due to their substantial contribution to *Chrnb2* expression across layers (Fig. 1H-I) and their known influence on PFC-dependent anxiety-like behavior (31). To achieve neuron- and region-specific KD via CRISPR, we crossed NPY-Cre mice with a Cre-dependent Cas9-GFP

line (19,20). In the NPY-Cre::Cas9-GFP mice, GFP expression largely matched adult NPY patterns in subcortical regions. However, in the cortex, it was more abundant, particularly in deep layers (Fig. 2A, B), consistent with transient developmental NPY promoter activity (32). In support of this hypothesis, FISH confirmed strong overlap between *Cre* and *Npy* mRNA (Fig. 2C, D) and minimal overlap between *Gfp* and *Npy* (Fig. 2E, F).

FISH-based cell-type analysis showed that ~70 % of GFP+ cells were excitatory (*Vglut1*+) and 30 % inhibitory (*Viaat*+). The inhibitory neurons were mostly represented by *Sst*+ neurons (16 %) and *Pv*+ neurons (13 %), which is in line with previous reports (16). To a lesser extent, we identified *Htr3a*+ neurons (2.1 %) and *Vip*+ neurons (1.4 %) (Fig. 2G-J). Thus, subsequent experiments targeted beta2* nAChRs in neurons with early expression of NPY (here labelled as eeNPY neurons), located mainly in deep layers and spanning both excitatory and inhibitory neuronal types.

To induce KD, NPY-Cre::Cas9-GFP mice were injected with AAV-sgRNA-*Chrnb2* (Fig. 3A-C), yielding expression across +2.8-+1.6 mm from bregma (Fig. 3A-C). Some mice showed unilateral expression but were retained in the study. The number of double-positive (GFP+mCherry+) cells did not differ between sgRNA-scr and sgRNA-Chrnb2 groups (Fig. 3D). To confirm the efficiency of our KD approach, we first measured the binding of beta2* nAChRs radioligand [3H]epibatidine in brain homogenates obtained from NPY-Cre::Cas9-GFP mice injected with sgRNA-Chrnb2 and sgRNA-scr. However, we could not detect any difference in the [3H]epibatidine binding between the control and sgRNA-Chrnb2 injected mice or even in beta2-fx/fx mice crossed with the NPY-Cre line, likely due to the low proportion of double-positive neurons in the homogenate (Fig. 3E). The [3H]epibatidine binding showed only a modest decrease in homogenates from beta2-flox/flox mice injected with AAV5-CMV-Cre vector, inducing beta2* nAChRs deletion in all transduced cells (Fig. 3E, right). This points to the fact that even after the complete deletion, the beta2* nAChRs expressed on terminals projecting from other brain regions remained intact. Given the absence of reliable beta2-targeting antibodies, we used the T7 endonuclease assay to confirm that CRISPR indels were present only in sgRNA-Chrnb2-injected homogenates (Fig. 3F).

KD of beta2* nAChRs in the eeNPY-Cre neurons leads to working memory impairment and changes in exploratory behavior

To test whether the selective KD leads to reproducible changes in behavior, we tested our control and mutant mice in a battery of behavioral tasks (Fig. 4A), probing potential changes in motor activity, exploratory behavior, working memory, social and anxiety-like behavior and passive coping behavior (Fig. 4C- H, Suppl. Fig. S4, Suppl. Fig. S5A-C). Two independent cohorts were analyzed to ensure reproducibility, and we present merged data for both cohorts as well as separate data for each individual cohort (green, blue and red graphs in Fig. 4 and Suppl. Fig. S4). We also found a potential effect of the NPY-IRES-Cre allele on the NPY expression (Fig. 4B). To avoid any confounding effects of altered NPY expression, only NPY-Cre heterozygotes were used.

The beta2* nAChRs KD in eeNPY-Cre neurons impaired working memory, as evidenced by reduced alternations in the Y-maze (Fig. 4C). Mutants also displayed increased interactions with the novel object in the NOR test across both cohorts (Fig. 4D), suggesting changes in exploratory behavior. Furthermore, changes in social behavior emerged, but they were less consistent: a modest increase in non-social preference was only apparent when data from both cohorts were pooled (Fig. 4E), and a similar effect, an increased interest in the object stimulus, was found only in cohort 2 in the social interaction test (Fig. 4G). In contrast, an increased interest in the novel social stimulus during the social memory test was observed only in cohort 1 (Fig. 4F). Finally, a strong anxiolytic phenotype in the EPM was observed in cohort 1 but not in cohort 2 (Fig. 4H).

All tested behavioral parameters were used in principal component analysis (PCA), and grouped based on their contributions to individual principal components. When transformed to PC scores, we found a significant difference in PC1 between control and mutant mice only for cohort 1 (Fig. 5A). In this cohort, the PC1 was primarily driven by variables derived from the EPM task, and thus, the difference was not reproduced in cohort 2. We also checked whether the differences between cohorts can be related to differences in the AAV transduction efficiency. We found that cohort 2 showed a significantly higher number of double-positive cells in the PFC, primarily in control animals (Fig. 5B). When we correlated selected behavioral parameters with the number of double-positive cells in control and mutant animals in both cohorts (Fig. 5C-E), we found a significant but indirect correlation between the number of double-positive cells and the number of interactions with a novel object in the NOR test in mutant mice (Fig. 5D).

Finally, given the inconsistent findings in the EPM test across cohorts, we tested a new cohort both before and after the AAV-sgRNA injection in selected tests (Fig. 5G-I, Suppl. Fig. S5D-H). In line

with previous findings, we found a minor increase in the preference for the object and for the novel mouse in the social preference and memory task (Suppl. Fig. S5D-G). Importantly, baseline anxiety differed between groups in the EPM, but reversed afterward, and only mutants showed significant pre- vs. post-injection shifts (Fig. 5G-I). These data indicate that beta2* nAChRs KD anxiety-like behavior, but the effect is complex and dependent on other variables, such as prior exposure to the environment. Overall, KD in eeNPY-Cre neurons produced reproducible impairments in working memory and altered exploratory behavior, while effects on social and anxiety-like behavior were more subtle, variable and sensitive to cohort-specific factors.

KD of beta2* nAChRs in the NPY-expressing striatal interneurons leads to changes opposite to those in the PFC KD

In contrast to abundant cortical expression, striatal Cas9-GFP expression was sparse and consistent with adult NPY patterns (Fig. 6A). Because ~6 % of striatal NPY interneurons express *Chrnb2* (22), we asked whether KD in this rare population can affect behavior. NPY-Cre::Cas9-GFP mice injected in the dorsal striatum underwent the same behavioral tests as the previous PFC cohorts (Fig. 6B). The beta2* nAChRs KD affected behavioral domains similar to those observed in the PFC cohorts. However, mutant mice showed changes mostly opposite to those observed after PFC KD (Fig. 6C-F, Suppl. Fig. S6): reduced object exploration in NOR (Fig. 6C), increased sociability in social preference (Fig. 6D) and an anxiolytic-like phenotype in the EPM (Fig. 6E, F). Working memory was unaffected (Suppl. Fig.6G).

KD of beta2* nAChRs in the 5HT3aR-expressing PFC neurons leads to partially overlapping but distinct behavioral changes

To test whether beta2* nAChRs in another PFC population contribute differently to behavior, we targeted Htr3a+ interneurons. As we showed previously (Fig. 1, Suppl. Fig. S1), *Htr3a*+ neurons have similar *Chrnb2* expression but they are sparser, and they show distinct layer distribution (17). We crossed the Htr3a-Cre mice (21) with the Cas9-GFP line (Fig. 7A). The Cre-GFP expression in Htr3a-Cre::Cas9-GFP mice in the PFC was very different from the expression observed in NPY-Cre::Cas9-GFP. The Cre-GFP-positive neurons were relatively rare; they were observed in all cortical layers, but in line with our FISH data (Fig. 1E), they showed a preference for the upper layers (Fig. 7A). Htr3a-Cre::Cas9-GFP mice received AAV-sgRNA injections and were tested behaviorally (Fig. 7B). The AAV-sgRNA (mCherry) expression was examined in all mice used

for behavior and double-positive cell counts were similar between groups (Fig. 7C). Beta2* nAChRs KD in 5HT3a+ neurons produced behavioral changes that were partially similar to those observed in NPY-Cre::Cas9-GFP mice but also showed some major differences (Fig. 7D-H, Suppl. Fig. S7A-P). Mutant mice showed a pronounced hypersocial phenotype, spending more time interacting with the social and less with non-social stimuli (Fig. 7D, E), which is opposite to the trend in eeNPY mutants (Fig. 4E, Suppl. Fig. S5F). Htr3a-Cre::Cas9-GFP mutants also showed increased engagement in the social interaction test (Fig. 7F). While social behavior showed opposing changes in the two mutants, exploration-related measures displayed similar trends: non-significantly reduced Y-maze alternation (Fig. 7G), and increased novel object interactions in NOR (Fig. 7H). Lastly, anxiety-like behavior remained unchanged (Suppl. Fig. S7K, L).

Discussion

In this study, we examined the expression and behavioral significance of beta2* nAChRs across several neuronal populations in the PFC and dorsal striatum. We showed that beta2* nAChRs are highly expressed in all major neuronal types in the PFC and that selective KD of these receptors produces partially overlapping yet distinct - and at times opposing - behavioral effects. Although the precise nature of these behavioral changes sometimes varied, the functional domains affected by beta2* nAChRs KD remained remarkably consistent across neuronal types and brain regions. In the PFC, beta2* nAChRs KD induced changes in working memory, exploratory behavior, social behavior and anxiety-like behavior. Striatal KD affected similar domains, except for working memory, consistent with the well-established role of the PFC, but not the dorsal striatum, in this cognitive function (33). By contrast, we detected no changes in motor activity, passive coping behavior or compulsive/stereotypic behavior.

Our FISH analysis demonstrated that beta2* nAChRs are expressed across all major neuronal types in the PFC, partly contrasting with conclusions from previous electrophysiological studies (6,12,34). Although mRNA detection does not guarantee the presence of functional receptors, our work provides the first systematic analysis of *Chrnb2* expression by the main PFC populations, revealing that a substantial proportion of these neurons expresses detectable levels of beta2 subunit mRNA. Importantly, the expression of *Chrnb2* within a given neuronal type was largely unaffected by cortical layer, remaining relatively stable across the cortical depth (Suppl. Fig. S1C). *Vip*+

neurons in layer VI were a notable exception, showing markedly higher *Chrnb2* expression. This may indicate the existence of subpopulations within the *Vip*+ class as previously proposed (30). We also observed substantial variability in *Chrnb2* expression within the *Sst*+ population across sections (Fig. 1H), but this variability did not correlate with bregma position or other identifiable parameters.

While *Chrnb2* expression remained stable within neuronal types across layers, the relative abundance of most neuronal types increased in deeper layers (Fig. 1E). Accordingly, in layer VI the examined neuronal types accounted for nearly all *Chrnb2*+ cells, whereas in superficial layers a considerable proportion of *Chrnb2*+ cells could not be assigned to the profiled populations (Fig. 1I). Technical factors, such as differences in probe sensitivity or limitations in image analysis, may partially contribute to this discrepancy. However, the proportion of unidentified *Chrnb2*+ cells suggests that additional, uncharacterized cell types may contribute to beta2* nAChRs expression in upper layers.

One unexpected observation in this study was the high prevalence of eeNPY neurons in deep cortical layers in the NPY-Cre::Cas9-GFP model. This aberrant cortical expression was not reported in the original characterization of this line (20), but similar findings have been noted elsewhere (32). We propose that this pattern reflects early developmental NPY promoter activity in neural progenitor cells that later give rise predominantly to deep-layer cortical neurons with prominent output connectivity. Whether and to what extent these eeNPY neurons constitute a functionally distinct population remains to be determined.

A central question of this study was whether more selective targeting of nAChRs could yield more efficient, precise and predictable control over behavioral and cognitive phenotypes. Our results show that selective receptor manipulations in different neuronal types or brain regions can indeed lead to divergent behavioral outcomes, including hyper- versus hypo-social phenotypes and opposing effects on anxiety-like behavior. Yet, despite these differences in directionality, the broader behavioral domains affected remained strikingly consistent. These recurrent alterations may reflect the pharmacological properties of beta2* nAChRs, including their affinity for acetylcholine (ACh). These properties may render them particularly responsive to ACh fluctuations controlled by particular task conditions, such as novelty and arousal state. Future studies should directly test how beta2* nAChRs-mediated behavioral control is modulated by

altered ACh levels, for example, by using acetylcholinesterase inhibitors. In addition, monitoring ACh dynamics during behavioral tasks, as performed in previous work (35), would also be highly informative. Because ACh levels vary with vigilance and arousal (36), fluctuations in these states may help explain why some anxiety and social measures differed across cohorts. Differences in baseline stress associated with distinct housing facilities, or subtle variations in the characteristics of social stimuli, may also have contributed. Moreover, because NPY release is itself stress-sensitive (37,38), nicotinic modulation of eeNPY neurons may exert distinct effects under different baseline stress conditions.

All behavioral domains affected by our receptor manipulations have previously been linked to nicotinic signaling (14,22,39–44). Notably, earlier studies reported that deleting beta2* nAChRs in the PFC produces a hypersocial phenotype (14), possibly mediated by alterations in GABAergic interneuron function (45). Intriguingly, we observed a similar hypersocial phenotype only when beta2* nAChRs were knocked down in Htr3a+ interneurons, whereas KD in eeNPY neurons increased preference for non-social stimuli. These divergent, neuronal-type-specific outcomes are particularly relevant to models of autism spectrum disorder (ASD), where disruptions in excitatory/inhibitory balance are commonly observed (46). Our findings suggest that therapeutic strategies targeting beta2* nAChRs may require neuronal-type-specificity to effectively correct social deficits. Importantly, even a sparse population of receptors can shape behavior, as indicated by the effects of beta2* nAChRs KD in striatal NPY interneurons, a population with low *Chrnb2* expression (22).

In conclusion, we demonstrated that even widely expressed neurotransmitter receptor subtypes, such as beta2* nAChRs, can exert distinct functional roles depending on the neuronal population in which they are expressed. This neuronal-type specificity should be taken into account when investigating receptor function and when designing targeted interventions to modulate behavior. Emerging technologies that integrate pharmacological and genetic approaches (47–49) can enable us to exploit the complexity of receptor expression and function in a neuronal-type-specific manner. Ultimately, such precision may open new avenues for selective, effective targeting of neurotransmitter receptors in clinical practice.

Acknowledgements

We thank Dr. Cecilia Gotti for her help with the [3H]epibatidine binding experiments. We thank Dana Ungerova for her technical assistance. This work was supported by the Czech Ministry of Education, Youth and Sport (MSMT), project ERC CZ LL2402. We acknowledge the Light Microscopy Core Facility, IMG, Prague, Czech Republic, supported by MEYS – LM2023050, MEYS – CZ.02.1.01/0.0/0.0/18_046/0016045 and MEYS – CZ.02.01.01/00/23_015/0008205, for their support with the imaging and image analysis presented herein. Supported also by IPHYS BIF – MEYS CR (Large RI Project LM2023050 Czech-BioImaging) and ERDF (Project No. CZ.02.1.01/0.0/0.0/18_046/0016045). We thank Marie-Laure Niepon of the Image Platform at the Institute of Vision in Paris, France, for scanning the FISH slides.

Author Contributions

A.A., S.D., V.B. and H.J. designed research. A.A., J.E., C.R.V., A.R.A.B., T.J.D., S.D. and H.J. performed research. A.A., C.R.V., A.R.A.B., M.C., A.G., S.D. and H.J. analyzed data. H.J. and C.R.V. wrote the paper. A.A. and V.B. edited the paper.

Conflict of Interests

Nothing to declare.

Data Availability

The data generated and analyzed in this study are available from the corresponding author upon request.

Figures and Figure legends

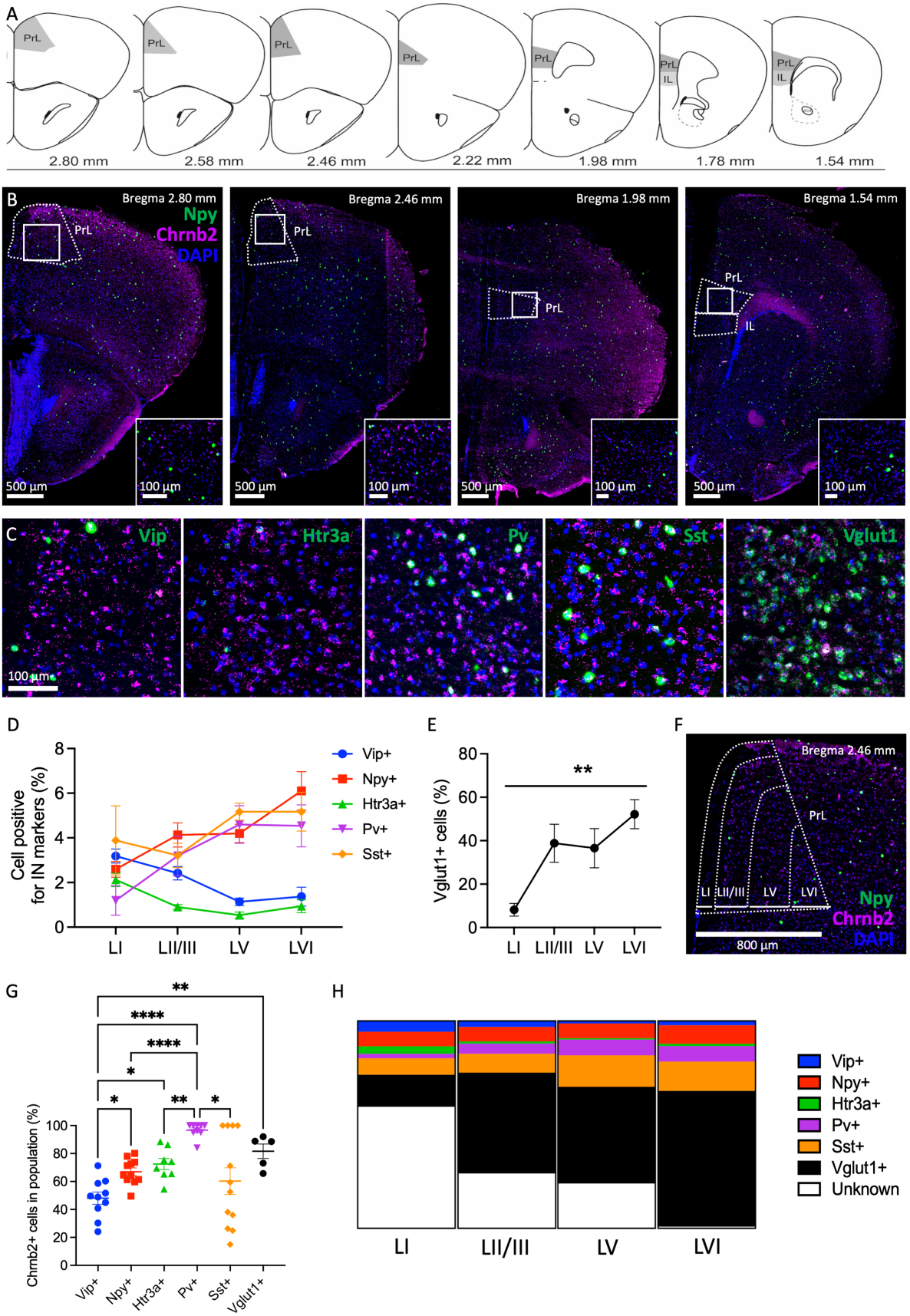
A
PrL
IL
2.80 mm
2.58 mm
2.46 mm
2.22 mm
1.98 mm
1.78 mm
1.54 mm
B
Bregma 2.80 mm
Bregma 2.46 mm
Bregma 1.98 mm
Bregma 1.54 mm
Npy
Chrnb2
DAPI
500 µm
100 µm
C
Vip
Htr3a
Pv
Sst
Vglut1
D
Cell positive for IN markers (%)
Vip+
Npy+
Htr3a+
Pv+
Sst+
LI
LII/III
LV
LVI
E
Vglut1+ cells (%)
**
F
800 µm
G
Chrnb2+ cells in population (%)
Vip+
Npy+
Htr3a+
Pv+
Sst+
Vglut1+
H
Vglut1+
Unknown

Figure 1

Expression of beta2* nAChRs by different neuronal populations of the mouse PFC. (A) Anatomical areas examined by the FISH analysis are highlighted in grey. (B) Examples of sections stained for *Npy/Chrnb2* colocalization, showing DAPI (blue), *Npy* (green), and *Chrnb2* (magenta). (C) Overlay images of *Chrnb2* probe (magenta) colocalized with probes for markers of individual neuronal populations (green): *Vip*, *Htr3a*, *Pv*, *Sst* and *Vglut1*. (blue: DAPI). (D) The percentage of cells positive for markers of the main inhibitory populations across PFC cortical layers. Layer vs. neuronal type interaction, $F_{(12, 179)}=2.96$, $p=0.0009$. Two-way ANOVA. (E) The percentage of cells positive for the excitatory marker *Vglut1* across PFC cortical layers. Main effect of layer: $F_{(3, 16)}=6.49$, **, $p=0.0044$. One-way ANOVA. (F) A scheme of four cortical layers in the medial PFC. (G) The percentage of cells expressing *Chrnb2* in the main PFC neuronal populations. Each symbol shows an average per section (averaged left and right hemisphere). Main effect of neuronal type, $F_{(5, 19)}=9.8$, $p<0.0001$. Welch's one-way ANOVA. *, $p<0.05$, **, $p<0.01$, ****, $p<0.0001$. Dunnett's multiple comparisons test. (H) The proportion of major PFC neuronal types out of all *Chrnb2*+ cells across PFC layers. PrL=prelimbic cortex, IL=infralimbic cortex.

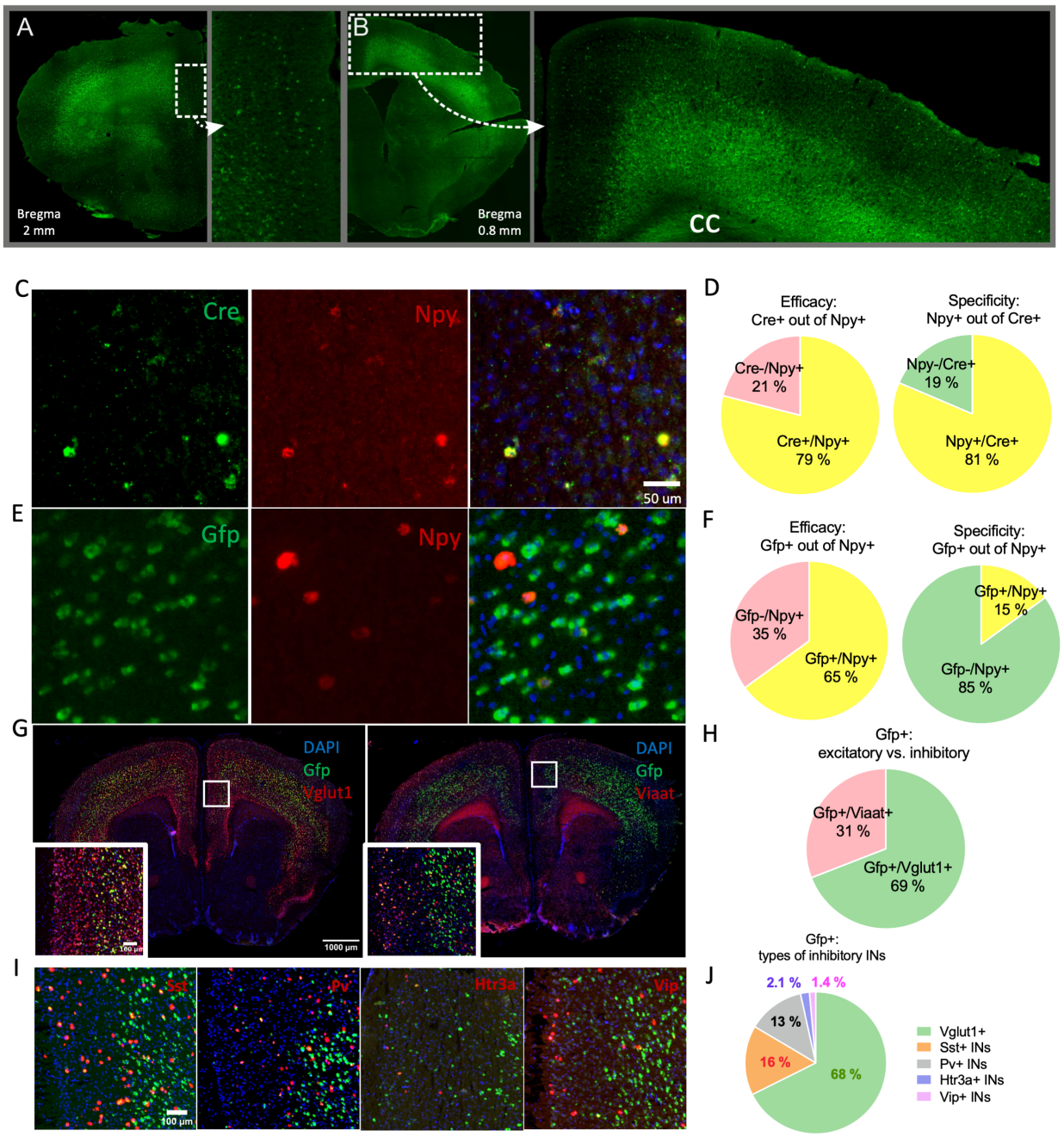

Figure 2

Characterization of the NPY-Cre mouse line. (A, B) Brain sections from NPY-Cre::Cas9-GFP mice showing widespread Cas-GFP expression in the cortex, primarily in layers V-VI. (C, D) Example of FISH images and quantification of the *Cre* and *Npy* mRNA colocalization, documenting a specificity of the NPY-Cre::Cas9-GFP model in adult mice. (E, F) Example of FISH images and quantification of the *Gfp* and *Npy* mRNA show modest overlap, indicating a

significant early Cre expression during development. (G) Example brain sections stained with FISH, showing Gfp (green) and Vglut1 or Viaat signal (red). (H) Proportion of excitatory and inhibitory neurons within the Cas9-GFP-expressing population. (I) Examples of FISH staining, showing Gfp (green) and the individual IN markers (left to right: Sst, Pv, Htr3a, Vip) (red). (J) Proportion of individual types of inhibitory INs within the Cas9-GFP-expressing population. cc=corpus callosum.

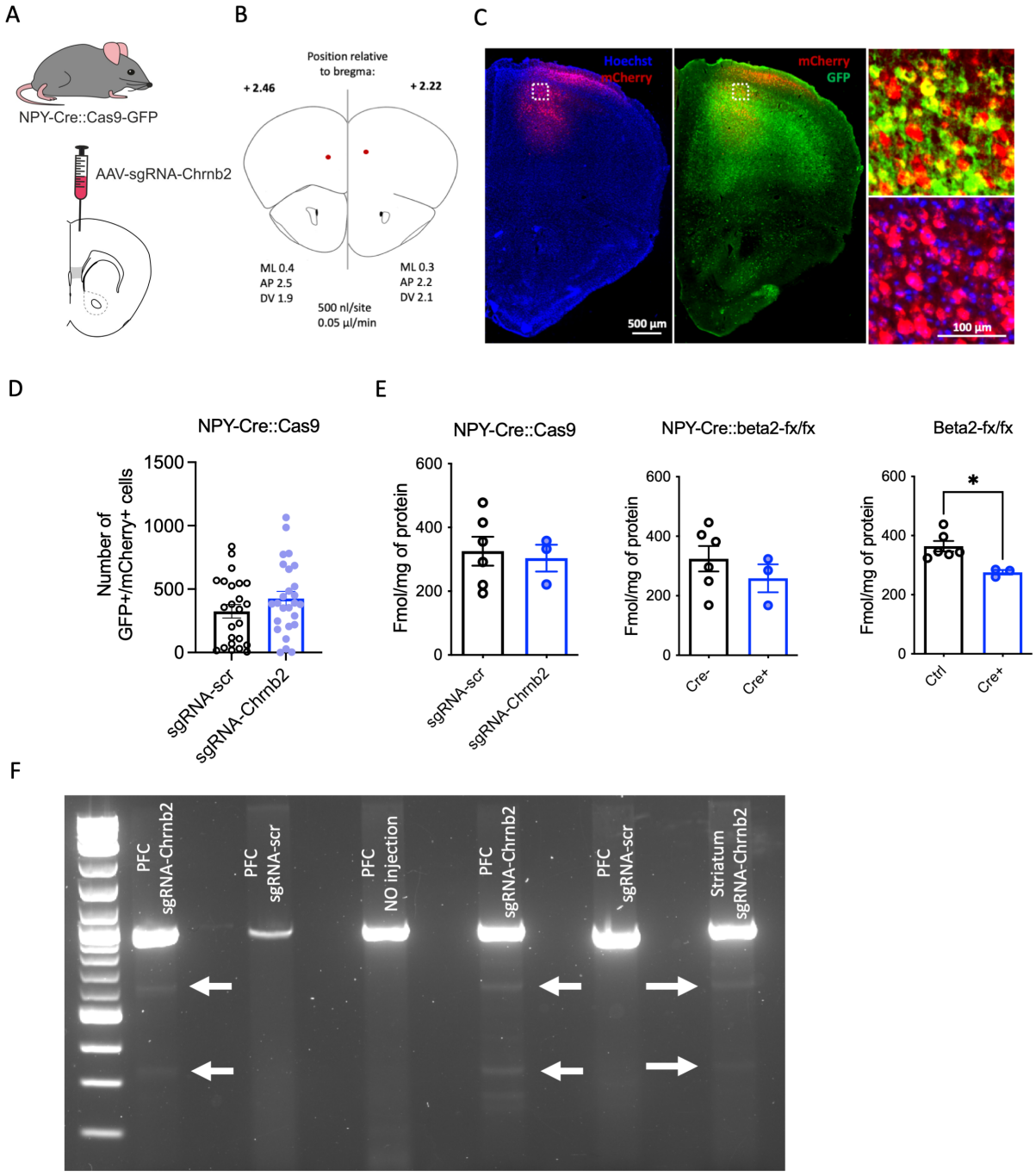

Figure 3

Evaluation of the KD of the beta2 nicotinic subunit induced by CRISPR. (A) A scheme of the KD strategy. (B) Stereotaxic coordinates and other parameters of the AAV-sgRNA injections. (C) An example of the AAV-sgRNA-Chrnb2 injected area. Left image and bottom close-up: Colocalization of the AAV-sgRNA vector (red) and nuclear staining (blue). Right image and top

close-up: Colocalization of the AAV-sgRNA vector (red) and Cas9-GFP (green) expression in the NPY-Cre mouse model. (D) Number of neurons double-positive for Cas9-GFP and AAV-sgRNA (mCherry) counted in sections from control (sgRNA-scr) and mutant (sgRNA-Chrnb2) NPY-Cre::Cas9-GFP mice that were used for behavioral analysis. Control vs. mutant mice, 95% CI for the difference between means [-88; 220], p=0.393, two-tailed t-test. (E) [3H]epibatidine binding in brain homogenates from NPY-Cre::Cas9-GFP mice injected with AAV-sgRNA-Chrnb2 (left), NPY-Cre::beta2-flox/flox mice (middle) and beta2-flox/flox mice injected with AAV-Cre (right). NPY-Cre::Cas9: ctrl vs. mutant mice, 95% CI for the difference between means [-192; 148], p=0.770. NPY-Cre::beta2-flox/flox: Cre- vs. Cre+ mice, 95% CI for the difference between means [-231; 100], p=0.379. Beta2-flox/flox: GFP- vs. Cre-GFP-injected mice, 95% CI for the difference between means [-151; -25], p=0.0132, all by two-tailed t-test. (F) Results of the T7 assay demonstrating CRISPR-induced mismatches in the *Chrnb2* gene. Means ±SEM are shown in all graphs. PFC=prefrontal cortex.

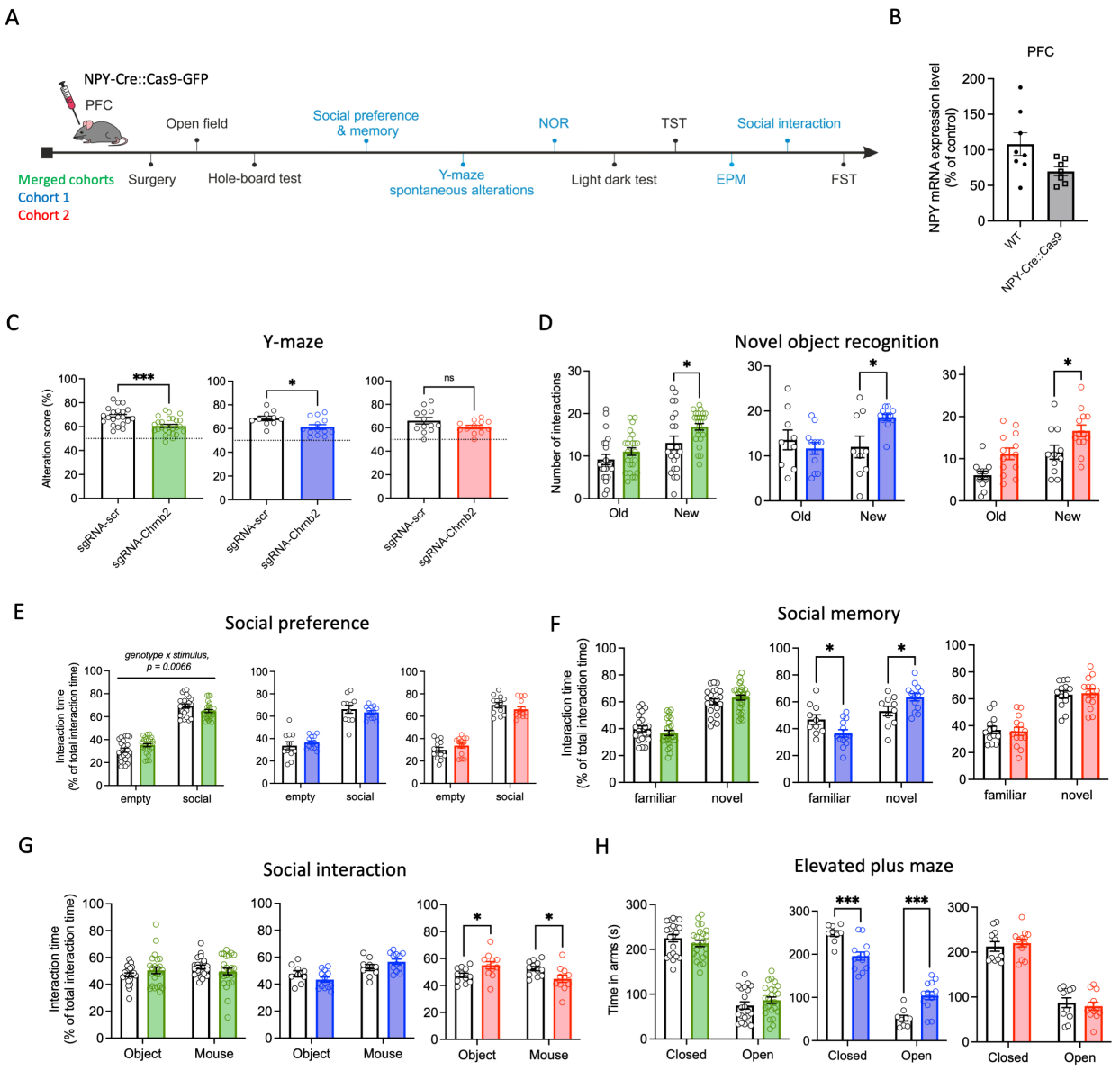

Figure 4

KD of beta2 nicotinic subunit in NPY-Cre-positive population leads to specific changes in behavior. (A) An overview and the order of behavioral tests performed in NPY-Cre::Cas-GFP mice injected with sgRNA-scr (controls) or sgRNA-Chrnb2 (mutants). Tests showing behavioral alterations in mutants are highlighted in blue color. (B) Expression of *Npy* mRNA in WT vs. NPY-Cre::Cas9-GFP mice. 95% CI for the difference between means [-77; 0.76], p=0.054, two-tailed t-test. (C-H) Results of tests showing behavioral alterations in NPY-Cre::Cas9-GFP mutant animals. All tests were performed in two independent cohorts. Pooled data are shown on the left (green

graphs, n(ctrl)=21-22, n(mutant)=24-27), cohort 1 in the middle (blue graphs, n(ctrl)=9-11, n(mutant)=12-13) and cohort 2 on the right (red graphs, n(ctrl)=11-13, n(mutant)=11-14). Means ±SEM are shown in all graphs. (C) Spontaneous alternations Y-maze test, alternation score in ctrl vs. mutant mice. Pooled cohorts: 95 % CI [-12.2; -3.9], p=0.0003. Cohort 1: 95 % CI [-13.2; -1.3], p=0.0199. Cohort 2: 95 % CI [-11.8; 1.0], p=0.096, all by two-tailed t-test. (D) Novel object recognition test, number of interactions in ctrl vs. mutant mice. Pooled cohorts, effect of genotype: $F_{(1, 88)}$=6.4, p=0.013; number of interactions with the new object in ctrl vs. mutant mice, p=0.036. Cohort 1, genotype x object interaction: $F_{(1, 38)}$=6.6, p=0.014; number of interactions with the new object in ctrl vs. mutant mice, p=0.015. Cohort 2, effect of genotype: $F_{(1, 44)}$=13, p=0.0007; number of interactions with the new object in ctrl vs. mutant mice, p=0.0258. Two-way ANOVA with Sidak's post hoc comparison test. (E) Social preference test, interaction time in ctrl vs. mutant mice, genotype x stimulus interaction. Pooled cohorts: $F_{(1, 94)}$=7.7, p=0.007. Cohort 1: $F_{(1, 44)}$=1.2, p=0.28. Cohort 2: $F_{(1, 50)}$=3.1, p=0.8. Two-way ANOVA. (F) Social memory test, interaction time in ctrl vs. mutant mice, genotype x stimulus interaction. Pooled cohorts: $F_{(1, 94)}$=2.4, p=0.1192. Cohort 1: $F_{(1, 42)}$=10, p=0.002. Cohort 2: $F_{(1, 50)}$=0.1, p=0.71. Two-way ANOVA. (G) Social interaction test, interaction time in ctrl vs. mutant mice, genotype x stimulus interaction. Pooled cohorts: $F_{(1, 88)}$=2.6, p=0.11. Cohort 1: $F_{(1, 38)}$=4, p=0.0506. Cohort 2: $F_{(1, 42)}$=12, p=0.0013. Two-way ANOVA. (H) Elevated plus maze, time in arms in ctrl vs. mutant mice, genotype x arm interaction. Pooled cohorts: $F_{(1, 86)}$=2.3, p=0.13. Cohort 1: $F_{(1, 40)}$=34, p<0.0001. Cohort 2: $F_{(1, 42)}$=0.5, p=0.45. Two-way ANOVA.

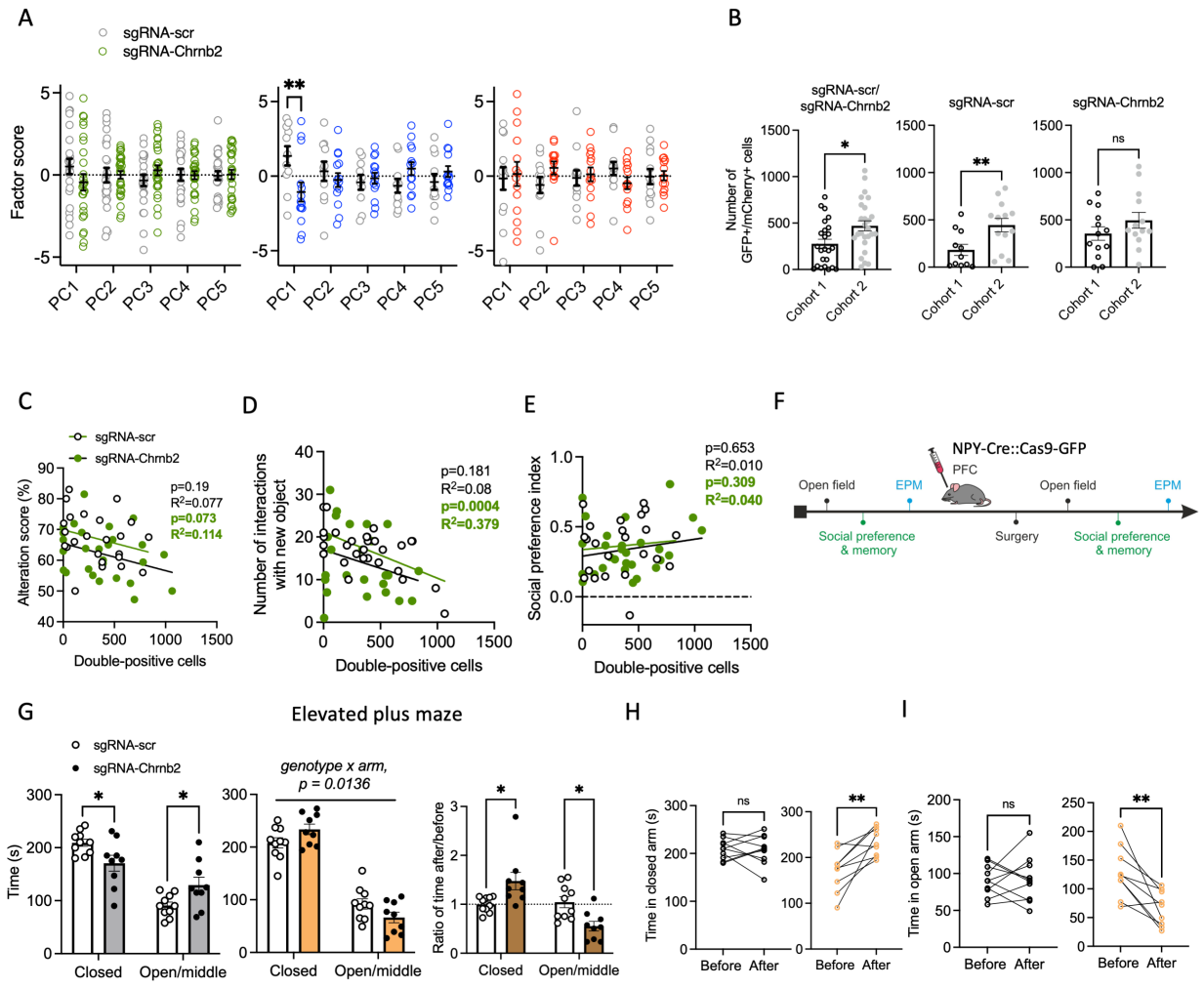

Figure 5

Interactions with the novel object are correlated with the number of AAV-transduced cells. (A) Behavioral data were transformed into factor scores by principal component analysis. The results are shown for behavioral data pooled from both cohorts (left, in green), and individually for cohort 1 (middle, in blue) and cohort 2 (right, in red). Factor scores for PC1 differ between the control and mutant mice only in cohort 1. Genotype x PC interaction, p=0.0059, $F_{(4, 114)}$=3.8, **, p<0.01. Two-way ANOVA with Sidak's post-hoc test. (B) Number of neurons double-positive for Cas9-GFP and AAV-sgRNA (mCherry) counted in sections from control (sgRNA-scr) and mutant (sgRNA-Chrnb2) NPY-Cre::Cas9-GFP mice that were used for behavioral analysis. Left: comparison of both sgRNA-scr and sgRNA-Chrnb2-injected mice pooled together (n(cohort 1)=24, n(cohort 2)=26). Cohort 1 vs. cohort 2, 95% CI for the difference between means [47; 341], p=0.011, Welch's t-test. Middle: comparison of control, sgRNA-scr-injected mice (n(cohort 1)=11,

n(cohort 2)=13). Cohort 1 vs. cohort 2, 95% CI for the difference between means [72; 453], p=0.0093, Welch's t-test. Right: comparison of mutant, sgRNA-Chrnb2-injected mice (n(cohort 1)=13, n(cohort 2)=13). Cohort 1 vs. cohort 2, 95% CI for the difference between means [-87; 368], p=0.214, Welch's t-test. (C-E) Selected behavioral parameters correlated with the number of double-positive cells in mice injected with sgRNA-scr or sgRNA-Chrnb2. Data from both cohorts are pooled. n(ctrl)=23, n(mutant)=30. (C) Spontaneous alternations in the Y-maze, alteration score correlated to the number of double-positive cells. Control mice: p=0.19, R^2=0.077, mutant mice: p=0.073, R2=0.114. (D) Novel object recognition test, number of interactions with the new object correlated with the number of double-positive cells. Control mice: p=0.181, R^2=0.080, mutant mice: p=0.0004, R^2=0.379. (E) Social preference test, social preference index correlated to the number of double-positive cells. Control mice: p=0.653, R^2=0.010, mutant mice: p=0.309, R^2=0.040. (F) An overview of experiments performed before and after the AAV-sgRNA injections. (G-I) Elevated plus maze test was performed both before and after the AAV-sgRNA injections. n(ctrl)=10, n(mutant)=9. (G) Left: Time spent in arms before the AAV-sgRNA injections. Genotype x arm interaction, p=0.0016, $F_{(1, 34)}$=12, *, p<0.05. Two-way ANOVA with Sidak's post-hoc test. Middle: Time spent in arms after the AAV-sgRNA injections. Genotype x arm interaction, p=0.014, $F_{(1, 34)}$=6.7. Two-way ANOVA. Right: Ratio of time spent in arms after vs. before the AAV-sgRNA injections. Genotype x arm interaction, p=0.0002, $F_{(1, 34)}$=18, *, p<0.05. Two-way ANOVA with Sidak's post-hoc test. (H) Comparison of time spent in closed arms before and after AAV-sgRNA injections in control (left) and mutant (right) mice. Controls before vs. after, 95% CI for the difference between means [-24; 21], p=0.9, paired t-test. Mutants before vs. after, 95% CI for the difference between means [26; 100], p=0.0043, paired t-test. (I) Comparison of time spent in open/middle arms before and after AAV-sgRNA injections in control (left) and mutant (right) mice. Controls before vs. after, 95% CI for the difference between means [-22; 24], p=0.9, paired t-test. Mutants before vs. after, 95% CI for the difference between means [-100; -26], p=0.0043, paired t-test.

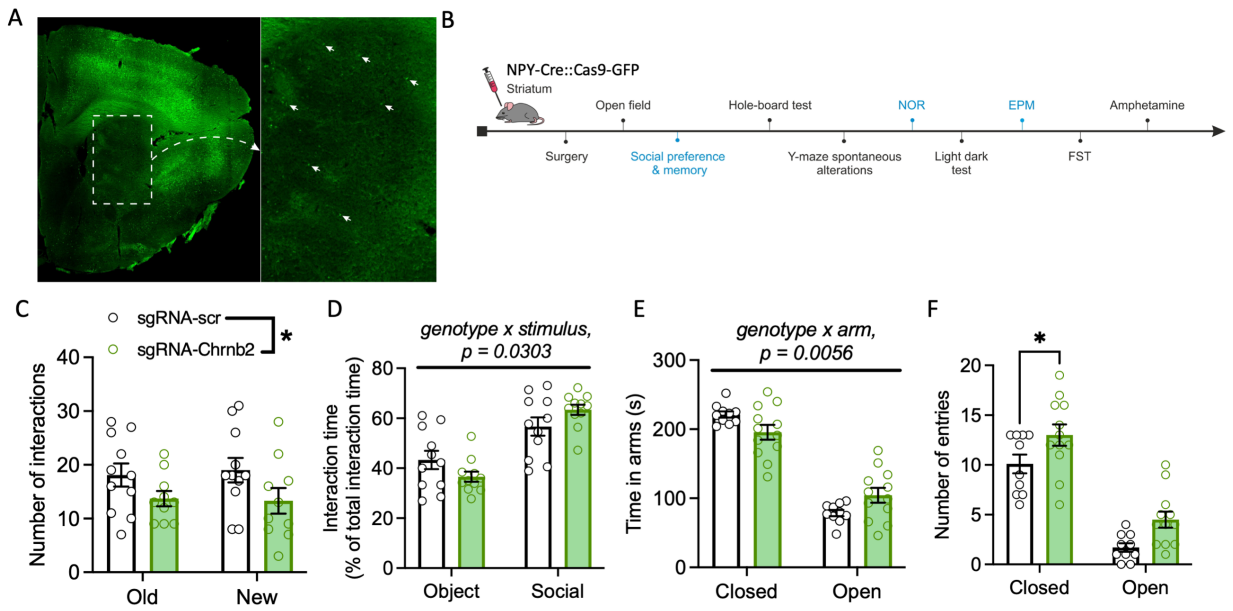

Figure 6

KD of beta2 nicotinic subunit in NPY-Cre-positive striatal neurons leads to changes in explorative, social and anxiety-like behavior. (A) A representative brain section from NPY-Cre::Cas9-GFP mouse showing scattered Cas-GFP expression in the DS. (B) An overview and the order of behavioral tests performed in NPY-Cre::Cas-GFP mice injected with sgRNA-scr (controls) or sgRNA-Chrnb2 (mutants). Tests showing behavioral alterations in mutants are highlighted in blue color. (C-F) Selected behavioral parameters in mice injected in the dorsal striatum with sgRNA-scr or sgRNA-Chrnb2. n(ctrl)=10-11, n(mutant)=10-12. (C) Novel object recognition test, number of interactions in ctrl vs. mutant mice. Effect of genotype: $F_{(1, 38)}$=5.6, p=0.022, two-way ANOVA. (D) Elevated plus maze, time spent in closed and open/middle arms in ctrl vs. mutant mice. Genotype vs. arm interaction: $F_{(1, 40)}$=8.5, p=0.0056, two-way ANOVA. (E) Elevated plus maze, number of entries in closed and open arms in ctrl vs. mutant mice. Effect of genotype: $F_{(1, 40)}$=11, p=0.0022. Number of entries in the closed arms in ctrl vs. mutant mice, p=0.047, number of entries in the open arms in ctrl vs. mutant mice, p=0.057. Two-way ANOVA followed by Sidak's post-hoc test. (F) Social preference test, percentage of time spent interacting with an object and social stimulus in ctrl vs. mutant mice. Genotype vs. stimulus interaction: $F_{(1, 40)}$=5, p=0.3. Two-way ANOVA.

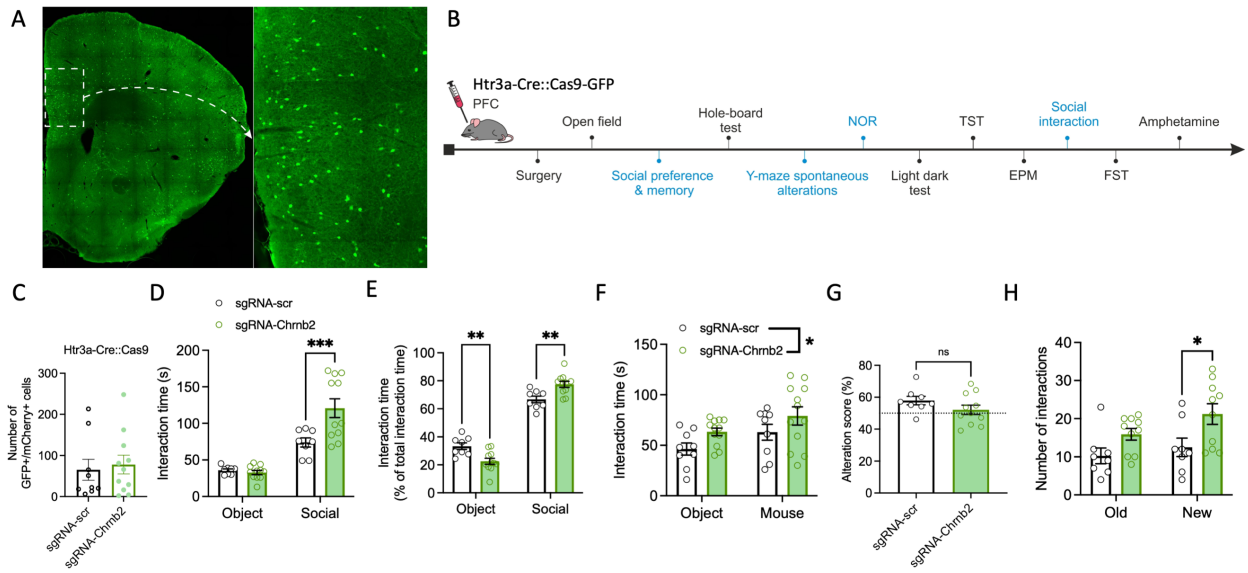

Figure 7

KD of beta2 nicotinic subunit in Htr3a-Cre-positive PFC neurons leads to higher sociability and exploration. (A) An overview and the order of behavioral tests performed in Htr3a-Cre::Cas-GFP mice injected with sgRNA-scr (controls) or sgRNA-Chrnb2 (mutants). Tests showing behavioral alterations in mutants are highlighted in blue color. (B) A representative brain section from Htr3a-Cre::Cas9-GFP mouse showing scattered Cas-GFP expression in the cortex, predominantly in superficial layers. (C) Number of neurons double-positive for Cas9-GFP and AAV-sgRNA (mCherry) counted in sections from control (sgRNA-scr) and mutant (sgRNA-Chrnb2) Htr3a-Cre::Cas9-GFP mice that were used for behavioral analysis. n(ctrl)=9, n(mutant)=11. 95% CI for the difference between means [-59; 85], p=0.71, two-tailed t-test. (D-H) Selected behavioral parameters in mice injected in the dorsal striatum with sgRNA-scr or sgRNA-Chrnb2. n(ctrl)=8-9, n(mutant)=10-12. (D) Social preference test, time spent interacting with an object and social stimulus in ctrl vs. mutant mice. Effect of genotype: $F_{(1, 34)}$=7, p=0.012. Genotype vs. stimulus interaction: $F_{(1, 34)}$=9, p=0.0048. Time spent with object in ctrl vs. mutant mice, p=0.96, time spent with social stimulus in ctrl vs. mutant mice, p=0.0006. Two-way ANOVA followed by post-hoc Sidak's test. (E) Social preference test, percentage of time spent interacting with an object and social stimulus in ctrl vs. mutant mice. Genotype vs. stimulus interaction: $F_{(1, 34)}$=21, p<0.0001. Percentage of time spent with object in ctrl vs. mutant mice, p=0.0045, percentage of time spent with social stimulus in ctrl vs. mutant mice, p=0.0045. Two-way ANOVA followed by post-hoc Sidak's test. (F) Y-maze test, alternation score in ctrl vs. mutant mice. 95%

CI for the difference between means [-14; 2.6], p=0.16, Welch's t-test. (G) Novel object recognition test, number of interactions with old and new object in ctrl vs. mutant mice. Effect of genotype: $F_{(1, 32)}$=10, p=0.0031. Number of interactions with old object in ctrl vs. mutant mice, p=0.16, number of interactions with new object in ctrl vs. mutant mice, p=0.02. Two-way ANOVA with post-hoc Sidak's test. (H) Social interaction test, time interacting with object and mouse stimuli in ctrl vs. mutant mice. Effect of genotype: $F_{(1, 38)}$=5.4, p=0.025. Two-way ANOVA.

References

1. Albuquerque EX, Pereira EFR, Alkondon M, Rogers SW. Mammalian nicotinic acetylcholine receptors: from structure to function. Physiol Rev. 2009 Jan;89(1):73–120.

2. Wittenberg RE, Wolfman SL, De Biasi M, Dani JA. Nicotinic acetylcholine receptors and nicotine addiction: A brief introduction. Neuropharmacology. 2020 Oct 15;177:108256.

3. Jensen AA, Frølund B, Liljefors T, Krogsgaard-Larsen P. Neuronal nicotinic acetylcholine receptors: structural revelations, target identifications, and therapeutic inspirations. J Med Chem. 2005 July 28;48(15):4705–45.

4. Zoli M, Pistillo F, Gotti C. Diversity of native nicotinic receptor subtypes in mammalian brain. Neuropharmacology. 2015 Sept;96(Pt B):302–11.

5. Terry AV, Jones K, Bertrand D. Nicotinic acetylcholine receptors in neurological and psychiatric diseases. Pharmacol Res. 2023 May;191:106764.

6. Poorthuis RB, Bloem B, Schak B, Wester J, de Kock CPJ, Mansvelder HD. Layer-specific modulation of the prefrontal cortex by nicotinic acetylcholine receptors. Cereb Cortex N Y N 1991. 2013 Jan;23(1):148–61.

7. Tasic B, Yao Z, Graybuck LT, Smith KA, Nguyen TN, Bertagnolli D, et al. Shared and distinct transcriptomic cell types across neocortical areas. Nature. 2018 Nov;563(7729):72–8.

8. Abbondanza A, Urushadze A, Alves-Barboza AR, Janickova H. Expression and function of nicotinic acetylcholine receptors in specific neuronal populations: Focus on striatal and prefrontal circuits. Pharmacol Res. 2024 June;204:107190.

9. Power SK, Venkatesan S, Lambe EK. Xanomeline restores endogenous nicotinic acetylcholine receptor signaling in mouse prefrontal cortex. Neuropsychopharmacol Off Publ Am Coll Neuropsychopharmacol. 2023 Mar;48(4):671–82.

10. Mineur YS, Soares AR, Etherington IM, Abdulla ZI, Picciotto MR. Pathophysiology of nAChRs: Limbic circuits and related disorders. Pharmacol Res. 2023 May;191:106745.

11. Koukouli F, Changeux JP. Do Nicotinic Receptors Modulate High-Order Cognitive Processing? Trends Neurosci. 2020 Aug;43(8):550–64.

12. Bloem B, Poorthuis RB, Mansvelder HD. Cholinergic modulation of the medial prefrontal cortex: the role of nicotinic receptors in attention and regulation of neuronal activity. Front Neural Circuits. 2014;8:17.

13. Proulx E, Piva M, Tian MK, Bailey CDC, Lambe EK. Nicotinic acetylcholine receptors in attention circuitry: the role of layer VI neurons of prefrontal cortex. Cell Mol Life Sci CMLS. 2014 Apr;71(7):1225–44.

14. Avale ME, Chabout J, Pons S, Serreau P, De Chaumont F, Olivo-Marin JC, et al. Prefrontal nicotinic receptors control novel social interaction between mice. FASEB J Off Publ Fed Am Soc Exp Biol. 2011 July;25(7):2145–55.

15. Koukouli F, Rooy M, Tziotis D, Sailor KA, O'Neill HC, Levenga J, et al. Nicotine reverses hypofrontality in animal models of addiction and schizophrenia. Nat Med. 2017 Mar;23(3):347–54.

16. Karagiannis A, Gallopin T, Dávid C, Battaglia D, Geoffroy H, Rossier J, et al. Classification of NPY-expressing neocortical interneurons. J Neurosci Off J Soc Neurosci. 2009 Mar 18;29(11):3642–59.

17. Lee S, Hjerling-Leffler J, Zagha E, Fishell G, Rudy B. The largest group of superficial neocortical GABAergic interneurons expresses ionotropic serotonin receptors. J Neurosci Off J Soc Neurosci. 2010 Dec 15;30(50):16796–808.

18. Burbridge TJ, Xu HP, Ackman JB, Ge X, Zhang Y, Ye MJ, et al. Visual circuit development requires patterned activity mediated by retinal acetylcholine receptors. Neuron. 2014 Dec 3;84(5):1049–64.

19. Platt RJ, Chen S, Zhou Y, Yim MJ, Swiech L, Kempton HR, et al. CRISPR-Cas9 knockin mice for genome editing and cancer modeling. Cell. 2014 Oct 9;159(2):440–55.

20. Milstein AD, Bloss EB, Apostolides PF, Vaidya SP, Dilly GA, Zemelman BV, et al. Inhibitory Gating of Input Comparison in the CA1 Microcircuit. Neuron. 2015 Sept 23;87(6):1274–89.

21. Gong S, Doughty M, Harbaugh CR, Cummins A, Hatten ME, Heintz N, et al. Targeting Cre recombinase to specific neuron populations with bacterial artificial chromosome constructs. J Neurosci Off J Soc Neurosci. 2007 Sept 12;27(37):9817–23.

22. Abbondanza A, Ribeiro Bas I, Modrak M, Capek M, Minich J, Tyshkevich A, et al. Nicotinic Acetylcholine Receptors Expressed by Striatal Interneurons Inhibit Striatal Activity and Control Striatal-Dependent Behaviors. J Neurosci Off J Soc Neurosci. 2022 Mar 30;42(13):2786–803.

23. Dumas S, Wallén-Mackenzie Å. Developmental Co-expression of Vglut2 and Nurr1 in a Mes-Di-Encephalic Continuum Preceeds Dopamine and Glutamate Neuron Specification. Front Cell Dev Biol. 2019;7:307.

24. Bankhead P, Loughrey MB, Fernández JA, Dombrowski Y, McArt DG, Dunne PD, et al. QuPath: Open source software for digital pathology image analysis. Sci Rep. 2017 Dec 4;7(1):16878.

25. Franklin KBJ, Paxinos G. The mouse brain in stereotaxic coordinates. Boston; 2008.

26. Peng C, Yan Y, Kim VJ, Engle SE, Berry JN, McIntosh JM, et al. Gene editing vectors for studying nicotinic acetylcholine receptors in cholinergic transmission. Eur J Neurosci. 2019 Aug;50(3):2224–38.

27. Swiech L, Heidenreich M, Banerjee A, Habib N, Li Y, Trombetta J, et al. In vivo interrogation of gene function in the mammalian brain using CRISPR-Cas9. Nat Biotechnol. 2015 Jan;33(1):102–6.

28. Lowry OH, Rosebrough NJ, Farr AL, Randall RJ. Protein measurement with the Folin phenol reagent. J Biol Chem. 1951 Nov;193(1):265–75.

29. Martinez-Marquez E, Reyes-Leon S, Garcia-San-Jose F, Lopez-Begines S, Nieto-Gonzalez JL, Garcia-Junco-Clemente P. Cholinergic Modulation of Chandelier Cells via Heteromeric Nicotinic Receptors in Prefrontal Cortex [Internet]. bioRxiv; 2025 [cited 2025 Nov 29]. p. 2025.01.18.633708. Available from: https://www.biorxiv.org/content/10.1101/2025.01.18.633708v1

30. Dellal S, Zurita H, Kruglikov I, Valero M, Abad-Perez P, Geron E, et al. Inhibitory and disinhibitory VIP IN-mediated circuits in neocortex [Internet]. bioRxiv; 2025 [cited 2025 Nov 29]. p. 2025.02.26.640383. Available from: https://www.biorxiv.org/content/10.1101/2025.02.26.640383v2

31. Saffari R, Teng Z, Zhang M, Kravchenko M, Hohoff C, Ambrée O, et al. NPY+-, but not PV+- GABAergic neurons mediated long-range inhibition from infra- to prelimbic cortex. Transl Psychiatry. 2016 Feb 16;6(2):e736.

32. Xie Z, Li D, Cheng X, Pei Q, Gu H, Tao T, et al. A brain-to-spinal sensorimotor loop for repetitive self-grooming. Neuron. 2022 Mar 2;110(5):874-890.e7.

33. Lara AH, Wallis JD. The Role of Prefrontal Cortex in Working Memory: A Mini Review. Front Syst Neurosci. 2015 Dec 18;9:173.

34. Guillem K, Bloem B, Poorthuis RB, Loos M, Smit AB, Maskos U, et al. Nicotinic acetylcholine receptor β2 subunits in the medial prefrontal cortex control attention. Science. 2011 Aug 12;333(6044):888–91.

35. Mineur YS, Mose TN, Maibom KL, Pittenger ST, Soares AR, Wu H, et al. ACh signaling modulates activity of the GABAergic signaling network in the basolateral amygdala and behavior in stress-relevant paradigms. Mol Psychiatry. 2022 Dec;27(12):4918–27.

36. Chebolu S, Dayan P, Lloyd K. Vigilance, arousal, and acetylcholine: Optimal control of attention in a simple detection task. PLoS Comput Biol. 2022 Oct;18(10):e1010642.

37. Reichmann F, Holzer P. Neuropeptide Y: A stressful review. Neuropeptides. 2016 Feb;55:99–109.

38. Casello SM, Flores RJ, Yarur HE, Wang H, Awanyai M, Arenivar MA, et al. Neuropeptide System Regulation of Prefrontal Cortex Circuitry: Implications for Neuropsychiatric Disorders. Front Neural Circuits. 2022;16:796443.

39. Phenis D, Vunck SA, Valentini V, Arias H, Schwarcz R, Bruno JP. Activation of alpha7 nicotinic and NMDA receptors is necessary for performance in a working memory task. Psychopharmacology (Berl). 2020 June;237(6):1723–35.

40. Valentine G, Sofuoglu M. Cognitive Effects of Nicotine: Recent Progress. Curr Neuropharmacol. 2018;16(4):403–14.

41. Maskos U, Molles BE, Pons S, Besson M, Guiard BP, Guilloux JP, et al. Nicotine reinforcement and cognition restored by targeted expression of nicotinic receptors. Nature. 2005 July 7;436(7047):103–7.

42. Maubourguet N, Lesne A, Changeux JP, Maskos U, Faure P. Behavioral sequence analysis reveals a novel role for beta2* nicotinic receptors in exploration. PLoS Comput Biol. 2008 Nov;4(11):e1000229.

43. Nguyen C, Mondoloni S, Le Borgne T, Centeno I, Come M, Jehl J, et al. Nicotine inhibits the VTA-to-amygdala dopamine pathway to promote anxiety. Neuron. 2021 Aug 18;109(16):2604-2615.e9.

44. Picciotto MR, Lewis AS, van Schalkwyk GI, Mineur YS. Mood and anxiety regulation by nicotinic acetylcholine receptors: A potential pathway to modulate aggression and related behavioral states. Neuropharmacology. 2015 Sept;96(Pt B):235–43.

45. Qi C, Sima W, Mao H, Hu E, Ge J, Deng M, et al. Anterior cingulate cortex parvalbumin and somatostatin interneurons shape social behavior in male mice. Nat Commun. 2025 May 4;16(1):4156.

46. Sohal VS, Rubenstein JLR. Excitation-inhibition balance as a framework for investigating mechanisms in neuropsychiatric disorders. Mol Psychiatry. 2019 Sept;24(9):1248–57.

47. Gruber TD, Krishnamurthy C, Grimm JB, Tadross MR, Wysocki LM, Gartner ZJ, et al. Cell-Specific Chemical Delivery Using a Selective Nitroreductase-Nitroaryl Pair. ACS Chem Biol. 2018 Oct 19;13(10):2888–96.

48. Shields BC, Yan H, Lim SSX, Burwell SCV, Cammarata CM, Fleming EA, et al. DART.2: bidirectional synaptic pharmacology with thousandfold cellular specificity. Nat Methods. 2024 July;21(7):1288–97.

49. Shields BC, Kahuno E, Kim C, Apostolides PF, Brown J, Lindo S, et al. Deconstructing behavioral neuropharmacology with cellular specificity. Science. 2017 Apr 7;356(6333):eaaj2161.